Materials and Design 183 (2019) 108157

Contents lists available at ScienceDirect

Materials and Design

journal homepage: www.elsevier.com/locate/matdes

Wire + Arc Additively Manufactured Inconel 718: Effect of post-deposition heat treatments on microstructure and tensile properties

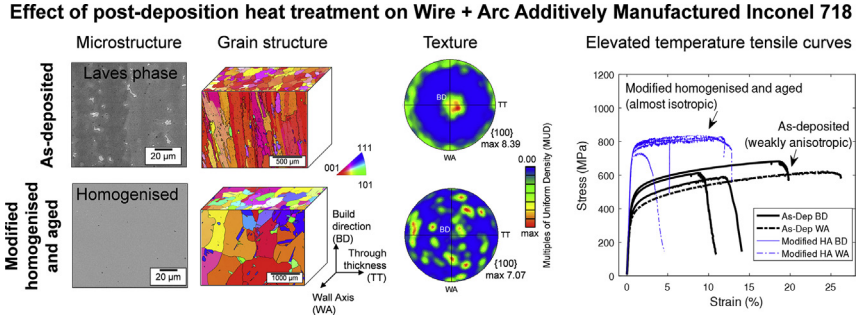
Cui E. Seow [a, b, *], Harry E. Coules [a], Guiyi Wu [c], Raja H.U. Khan [c], Xiangfang Xu [d], Stewart Williams [d]

[a] Department of Mechanical Engineering, University of Bristol, Bristol, BS8 1TR, UK
[b] NSIRC, TWI Ltd, Granta Park, Great Abington, Cambridge, CB21 6AL, UK
[c] TWI Ltd, Granta Park, Cambridge, CB21 6AL, UK
[d] Welding Engineering and Laser Processing Centre, Cranfield University, Cranfield, MK43 0AL, UK

HIGHLIGHTS

- As-deposited Wire + Arc Additively Manufactured (WAAM) Inconel (IN) 718 contains Laves phase in the microstructure.
- A modified post-deposition heat treatment successfully dissolved Laves phase without precipitating δ phase.
- Changes to the grain structure through heat treatments reduced anisotropy in elevated temperature tensile properties.
- Elevated temperature tensile properties of WAAM IN 718 meet minimum specifications for cast but not for wrought material.

GRAPHICAL ABSTRACT



ARTICLE INFO

Article history:
Received 11 June 2019
Received in revised form
19 August 2019
Accepted 23 August 2019
Available online 24 August 2019

Keywords:
Additive manufacturing
Nickel-base superalloy
Heat treatment
Microstructure
Tensile properties
Elevated temperature

ABSTRACT

Wire + Arc Additive Manufacturing (WAAM) can be used to create large free-form components out of specialist materials such as nickel-base superalloys. Inconel (IN) 718 is well suited for the WAAM process due to its excellent weldability. However, during deposition, WAAM IN718 is susceptible to micro-segregation, leading to undesirable Laves phase formation in the interdendritic regions. Further, the WAAM process encourages columnar grain growth and the development of a strong fibre texture, leading to anisotropy in grain structure. This unfavourable microstructure can be addressed through specialised post-deposition homogenisation heat treatments. A new modified heat treatment was found to be effective in dissolving Laves phase, whereas a standard treatment precipitated δ phase. Tensile test results revealed that Laves and δ phases lead to low ductility when present in a precipitation-hardened matrix. The modified heat treatment also reduced the anisotropy in grain structure, leading to almost isotropic elevated temperature tensile properties, which meet minimum specifications for conventional cast but not for wrought material. Specialised post-deposition heat treatments, which address the unique microstructure of WAAM IN718, are crucial to achieving optimal mechanical properties.

© 2019 The Authors. Published by Elsevier Ltd. This is an open access article under the CC BY license (http://creativecommons.org/licenses/by/4.0/).

1. Introduction

Wire + arc additive manufacturing (WAAM) is a directed energy deposition (DED) technique [1]. It uses an electric arc to simultaneously melt and deposit metal wire onto a substrate, thereby

* Corresponding author.
E-mail address: cuier.seow@bristol.ac.uk (C.E. Seow).

https://doi.org/10.1016/j.matdes.2019.108157
0264-1275/© 2019 The Authors. Published by Elsevier Ltd. This is an open access article under the CC BY license (http://creativecommons.org/licenses/by/4.0/).

building up a part layer by layer. Unlike powder-based manufacturing methods, WAAM can be used to build large parts quickly, due to its higher deposition rates. WAAM builds are near-net shape, which reduces machining operations and material wastage in comparison to traditional manufacturing methods of machining from a casting or forging. One study demonstrated that for an external landing gear assembly, the technique can provide material savings of up to 220 kg per part [2]. The cost-effectiveness of WAAM is multiplied when used with expensive materials such as titanium alloys and nickel-base superalloys. A fundamental property that determines a material's suitability to WAAM is weldability. One of the most weldable nickel-base superalloys is Inconel (IN) 718. Its low Ti and Al contents decrease its susceptibility to strain age cracking [3]. It is a precipitation hardenable superalloy known for its high-temperature strength and is widely used in the aerospace, nuclear, oil and gas industries. The alloy is hardened predominantly by a body-centred tetragonal phase, gamma double-prime, γ" (Ni_3Nb), which is typically precipitated in post-process aging treatments [4,5].

Deposition of IN718 using WAAM techniques has been demonstrated to be viable in several studies using metal-inert-gas (MIG) [6], tungsten-inert-gas (TIG) [7–9] and cold metal transfer (CMT) [10], although careful control of build parameters is necessary to prevent porosity and crack-like defects. In the as-deposited condition, WAAM IN718 has a dendritic microstructure decorated with Laves phase $(Ni,Cr,Fe)_2(Nb,Mo,Ti)$ and carbides [6–10]. Laves phase is generally deemed detrimental for mechanical properties, as its formation depletes the matrix of Nb for γ" precipitation and its presence may have an embrittling effect on the material. There are two possible ways of dealing with Laves phase – (i) preventing its formation during deposition, and (ii) dissolving it back into the matrix through homogenisation heat treatments. The formation of Laves phase, due to elemental segregation of heavier elements into the interdendritic regions, is governed by thermal conditions during deposition. At present, this is difficult to monitor and control due to the complex thermal cycling that the part undergoes during the WAAM process [11]. Therefore, post-deposition heat treatment is currently the most viable way of managing Laves phase in the as-deposited microstructure. However, standard heat treatment schedules, which are designed for cast or wrought IN718, may not be suitable for WAAM materials as they have a different starting microstructure.

The mechanical properties of WAAM materials at elevated temperature are especially important for IN718 since this material is most commonly used for high temperature applications. Whilst tensile properties of WAAM IN718 at room temperature have been shown to be comparable to cast material [8] but short of wrought material [10], the properties at elevated temperature remain largely unknown.

WAAM IN718 in the as-deposited condition has been found to have large columnar grains and a strong crystallographic texture [9,10]. Unlike fine-grained polycrystalline wrought materials, the grain structure of WAAM IN718 is highly anisotropic which could lead to direction dependent mechanical properties. It is important to assess the extent of anisotropy and reveal the relationship between the grain structure and mechanical properties, as knowledge of this structure-property relationship is critical in understanding the underlying mechanisms which govern the mechanical behaviour of WAAM materials. Although separate tensile properties for WAAM IN718 loaded in different directions have been reported [10], the extent of their anisotropy has not been quantified, and their relationship with the anisotropic grain structure remains unclear.

Post-deposition heat treatment can be a convenient way of improving the microstructure and grain structure of WAAM materials. However, little is known about the effects of heat treatments on grain size and texture, and the resulting mechanical properties of WAAM IN718. Although the use of high-pressure cold rolling [12–14] has been found to mitigate the formation of large columnar grains through recrystallisation, rolling requires expensive tooling, increases overall deposition time, places additional limitations on part geometry, and the levels of recrystallisation could vary across the height of the build [15]. Therefore, alternative ways of improving the grain structure of as-deposited material must be developed and the resulting direction dependency on mechanical properties must be examined.

In this work, the effectiveness of heat treatments in improving the microstructure and tensile properties of WAAM IN718 material was investigated, and the extent of anisotropy in tensile properties in relation to its microstructure was assessed. This was performed by comparing the (i) microstructure, (ii) grain size and texture, (iii) tensile properties at room and elevated temperature, of WAAM IN718 material in both the as-deposited and heat-treated conditions.

2. Methodology

2.1. WAAM wall manufacture and sample extraction

A WAAM wall specimen was built using a Migatronic 320 A AC/DC plasma controller with a water-cooled plasma torch in an argon filled glove box, as shown in Fig. 1. Purified argon was used to produce the plasma and for shielding. The position of the torch was controlled using a three-axis linear CNC system. IN718 wire, manufactured by INCO Alloys Limited, with diameter of 1.2 mm and chemical composition detailed in Section 2.5, was guided through a jig to the tip of the torch.

Each layer of the WAAM wall was deposited in an oscillating pattern about the wall axis. WAAM build parameters were selected based on previous work by Xu et al. [15]. The distance from the torch to the deposition surface was maintained at 8 mm. The current used was 240 A for the initial layers and was gradually decreased to 200 A after 18 layers. The torch travel speed was 6.5 mm/s, and the wire feed speed was adjusted between 1.5 and 2 m/min. The final build dimensions are 300 mm length by 27 mm thickness by 68 mm height (Fig. 2). No defects were observed from X-ray radiographs of the wall, although the minimum detectable size is 1.2 mm. Metallographic slices and cylindrical tensile specimens were extracted from the wall as shown in Fig. 2.

2.2. Heat treatment strategies

Heat treatments were performed using a vacuum furnace. The samples were positioned near the centre of the furnace chamber, using a stainless steel jig assembly. Samples were placed on a ceramic tile alongside titanium getters. Two thermocouples were placed in contact with the jig assembly to measure the internal temperature during the heat treatment. A photograph of the setup

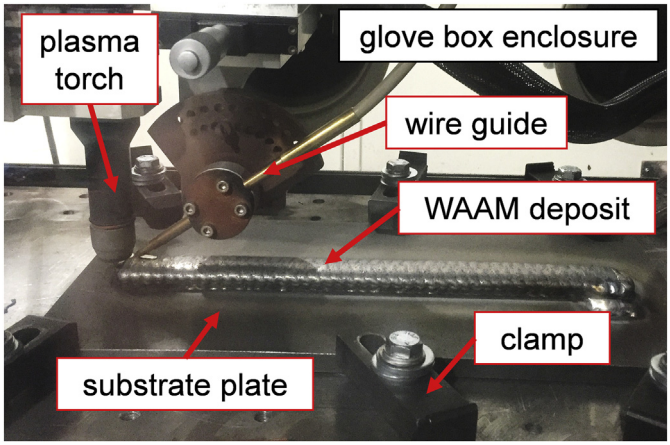


Fig. 1. WAAM equipment setup within the glove box.

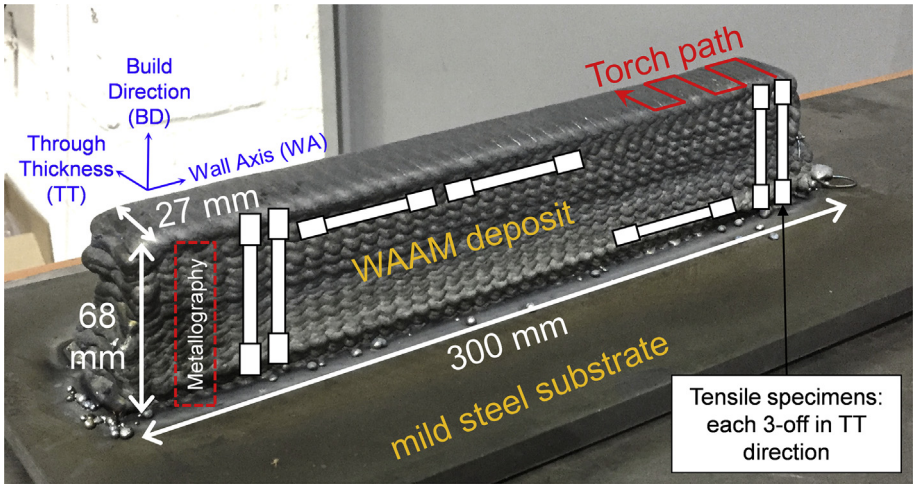


Fig. 2. Photograph of IN718 WAAM wall labelled with build dimensions, direction axes, oscillating torch path and extraction locations of metallographic slice and tensile specimens.

is shown in Fig. 3.

Two separate homogenisation treatments were investigated, (i) AMS 5383 [16] homogenisation treatment at 1100 °C for 1 h, air cool, and solution treatment at 980 °C for 1 h, air cool (Standard HSA) and (ii) a modified homogenisation treatment at 1186 °C for 40 min, air cool (Modified HA). The latter treatment is a novel modification of the homogenisation treatment of AMS 5383 [16], designed based on the Laves phase eutectic temperature at 1185 °C [17,18], used here for the first time on WAAM IN718 material. The modified homogenisation treatment also has a shorter hold time to reduce grain growth. Both treatments were followed by a standard double aging treatment, (720 °C for 8 h, furnace cool, and 620 °C for 8 h, air cool). In addition, one set of samples were aged without any homogenisation or solution treatment (Aging only). The temperature traces for the Standard HSA and Modified HA materials are shown in Fig. 4.

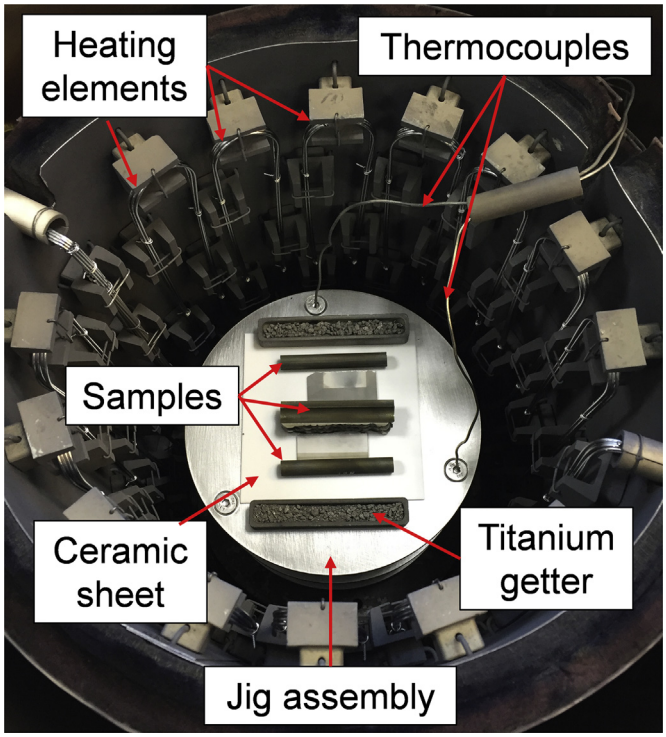


Fig. 3. Internal chamber of vacuum furnace used to perform heat treatments.

2.3. Metallographic preparation and analysis

Metallographic specimens were mounted, ground and polished to 0.25 μm. They were etched electrolytically with 20% H_2SO_4 at 3 V for 10 s. For Electron Backscatter Diffraction (EBSD), samples were given a final polishing with colloidal silica suspension. Light micrographs were taken using an optical microscope. Backscatter electron (BSE) images were taken using a ZEISS EVO Scanning Electron Microscope (SEM). Energy Dispersive X-ray Spectroscopy (EDX) analysis was also conducted using the SEM with an accelerating voltage of 20 keV. Point analyses were performed using a spot size of 1 μm. EBSD analyses were performed using a ZEISS SIGMA Field Emission Gun SEM and an Oxford Instruments Nordlys detector, with an accelerating voltage of 30 keV, aperture of 60 μm and step sizes between 3 and 5 μm.

2.4. Hardness and tensile testing methods

Vickers hardness testing was performed in compliance with BS EN ISO 6507-1 [19], using a load of 10 kg. Measurements were made at varying distances from the substrate. Standard tensile tests were performed to BS EN ISO 6892-1 [20] at room temperature and BS EN ISO 6892-2 [21] at 650 °C. For the latter, a high temperature extensometer was used to measure strain. Elongation at 650 °C was determined using the total length of the specimen, as gauge markings were masked by the discolouration of specimen surface during the high temperature test.

2.5. Characterisation of wire feedstock

The chemical composition of the IN718 wire feedstock is within the specifications of SAE International AMS5383 [16] and AMS5662 [22], as shown in Table 1, measured using Inductively Coupled Plasma Optical Emission Spectroscopy (ICP-OES) for major elements and inert gas fusion elemental analysis for C, N and O. Ti- and Nb-rich inclusions were found in the wire cross section, as shown in the Backscatter Electron (BSE) image and corresponding EDX spectra in Fig. 5. Spot 1 is likely to be a carbo-nitride containing both Ti and Nb, whose morphology and elemental composition is discussed further in Section 3.1.2. Spot 2 is likely to be MC-type carbide NbC, which is typically found in IN718. The distribution of the particles in the wire (streaks aligned with the wire axis) suggest that they might have been introduced during thermomechanical processes, such as rolling or extrusion, which are commonly used in wire production.

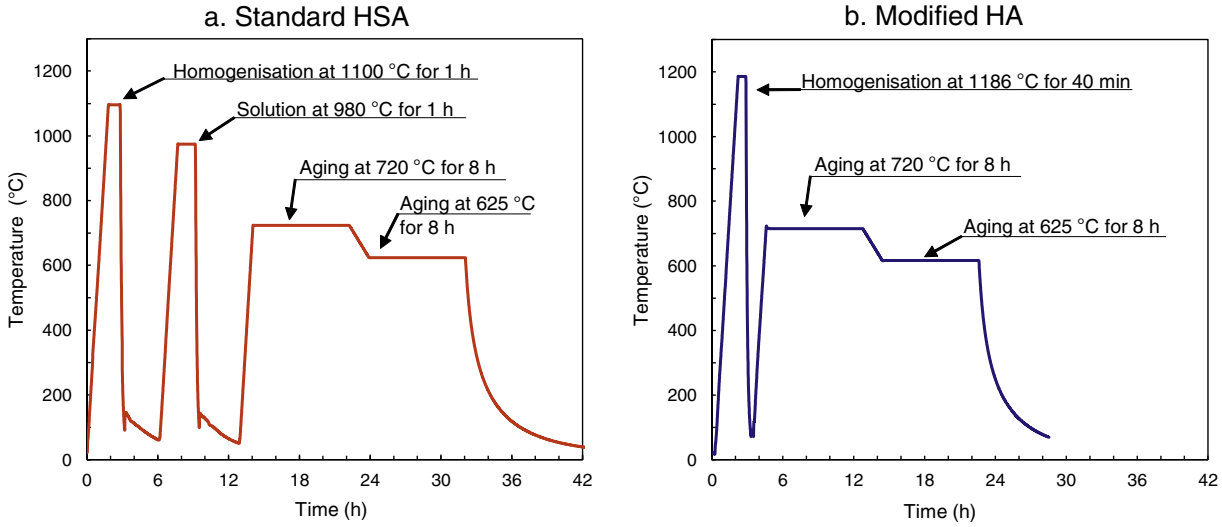


Fig. 4. Measured temperature traces for (a) standard homogenised and solution-aged and (b) modified homogenised and aged WAAM IN718 materials.

3. Results

3.1. As-deposited microstructure

3.1.1. Interlayer boundaries and dendritic microstructure

The as-deposited (As-Dep) WAAM IN718 etched metallographic specimen (Fig. 6) revealed alternating light and dark bands which seem to correlate with newly deposited material and re-heated zones. The interface between the bands is referred to as the interlayer boundary. The macrograph insert (Fig. 6) also shows epitaxial dendrite growth from the substrate plate generally in line with the build direction, indicating that the thermal gradient is the largest in this direction. Some dendrites have grown across interlayer boundaries and can be several millimetres long. The interlayer boundaries were observed to correspond to differences in dendrite patterns in the light micrographs (Fig. 7), but may be also be caused by a combination of weak segregation banding and solute partitioning in the heat affected zones, which has been recently observed in WAAM titanium alloys [23]. The curvature of the interlayer boundaries in Fig. 6 and Fig. 7 is likely to be partially due to the spreading of the molten pool towards the edge during deposition. The slightly outward-angled dendrite growth direction at the edges of the sample (shown in Fig. 7a and c) suggests that there was a small shift in the thermal gradient, which could be due to heat dissipation from the edges of the deposit.

3.1.2. Laves phase, inclusions and carbides

Laves phase, along with Ti- and Nb-rich inclusions (also found in the wire feedstock described in Section 2.5), were found in the As-Dep microstructure. The contrast of the SEM BSE images (Fig. 8a), which is contributed by topography and elemental differences [24], show particle morphology and elemental contrast in the microstructure. Elements in the phase particles were identified from EDX spot analysis spectra (Fig. 8b). The main elements in the γ-matrix, which is represented by Area 1 in Fig. 8a, are Ni, Cr and Fe, as shown by their large peaks in the corresponding spectrum in Fig. 8b. Smaller peaks were observed for Nb and Mo, as would be normally expected for IN718, whose chemical composition is detailed in Section 2.5.

Laves phase, appearing as light spots with island-like morphology (Spot 2 in Fig. 8a), were found to be richer in Nb and Mo than the matrix, inferred from the larger Nb and Mo peaks in Spectrum 2. These observations of Laves phase are consistent with those reported in observations of direct laser deposited IN718 [25], where the authors have confirmed the identity of Laves phase using Transmission Electron Microscopy (TEM). The presence of Laves phase is evidence of elemental segregation caused by a high heat input and slow cooling rate [26] during WAAM deposition. The role of Laves phase in mechanical properties, and strategies to mitigate its formation are discussed in Section 4.1.

Ti- and Nb-rich inclusions, have block-like morphology and can appear as dark or light spots (Spots 3 and 4 in Fig. 8a) depending on their proportions of Ti and Nb (dark spots are richer in Ti than Nb and vice versa). The smaller peaks in Spectra 3 and 4 are likely to have been contributed by the matrix, as the minimum spot size for EDX analysis (1 μm) is larger than the particles in Spots 3 and 4. Spot 4 in particular appears to be a Ti-rich core with a Nb-rich shell, consistent with TEM observations of similar particles in IN625 fusion welds [27], which the authors identified to be carbo-nitrides with a TiN core and NbC shell. TiN particles can act as nucleation sites for the formation of carbides like NbC [28,29], resulting in this type of complex particles. NbC is expected in the microstructure as it forms before Laves phase in the IN718 solidification sequence [30]. In contrast, TiN is likely to have come from the wire feedstock as its melting point (2950 °C [31]) is much higher than the temperature of the melt pool, therefore remains in the solid state throughout the WAAM deposition. This type of Ti- and Nb-rich carbo-nitride has also been previously reported in various IN718 materials: WAAM [10,15], cast ingots [32] hot-rolled bars [33], fusion welds [34] and claddings [35], indicating that these inclusions may have come from melting or thermomechanical processes commonly used to produce IN718 products.

3.2. Effect of heat treatment

3.2.1. Heat-treated microstructures

One purpose of the heat treatments is to dissolve Laves phase into the matrix. To this end, the starting WAAM IN718 microstructure has

Table 1
Chemical composition of INCO Alloy IN718 wire (wt%).

Element	Ni	Cr	Fe	Nb	Mo	Al	Ti	C	N (ppm)	O (ppm)
Composition	53.54	19.31	17.16	4.88	3.02	0.53	1.03	0.03	112	<50

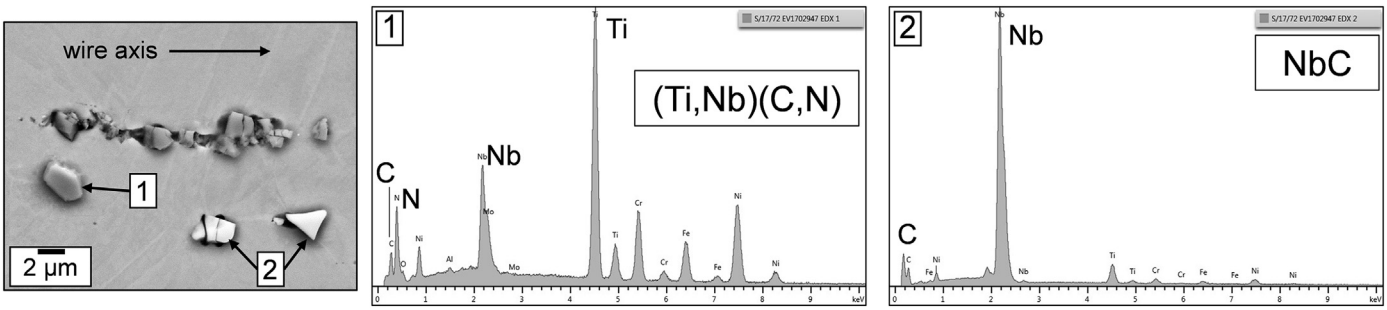


Fig. 5. SEM backscatter electron image and corresponding EDX spectra showing TiN and NbC particles in the wire feedstock.

responded well to both the Standard HSA and Modified HA treatments, as shown by the BSE micrographs in Fig. 9a and b respectively, which show little to no trace of Laves phase in the microstructures. Laves dissolves by diffusion of atoms into the matrix, at a rate dependent on the temperature and hold time of the homogenisation treatment [18]. Without any homogenisation treatment, the Aging only BSE micrograph (Fig. 9c) looks more similar to that of As-Dep WAAM IN718 (Fig. 8a), with Laves phase largely unchanged. This is due to the lower temperatures in the aging treatment, which are insufficient for dissolving Laves phase into the matrix.

However, the Standard HSA treatment also precipitated δ phase, whose identity has been inferred from its needle-like morphology and location at the grain boundaries, as shown in Fig. 9a. Similar observations of δ phase have been made in forged IN718 by Valle et al. [36], who confirmed using TEM diffraction patterns that δ phase has a needle-like morphology, which can be clearly distinguished from spherical γ' and elliptical γ". In wrought IN718, the precipitation of δ occurs between 860 °C to 995 °C [37] and requires Nb content of around 6–8% [38]. This implies that δ phase is likely to have precipitated during the 980 °C, 1 h solution treatment, which has been observed in selectively laser melted IN718 [39,40]. In addition, the dissolution of Laves phase during the homogenisation treatment may have created Nb-enriched regions in the microstructure, at which δ is more likely to precipitate. This has been previously observed in 980 °C, 1 h solution treated WAAM IN718 (no homogenisation treatment) [10,15], with δ phase precipitation around partially dissolved Laves phase. The acceptance of δ phase in the microstructure is dependent on several factors, which are discussed in Section 4.2. Ti and Nb-rich particles were found to remain in the heat-treated microstructures. Ti-rich nitrides and Nb-rich carbides are unlikely to be affected significantly by these heat treatments as their saturation-solubility [29] and eutectic [30] temperatures are higher than the treatment temperatures.

3.2.2. Heat-treated hardness and tensile properties

Another purpose of the heat treatments is to strengthen WAAM IN718 through precipitation hardening. Whilst the three heat-treated samples have undergone the same aging treatment, their response may differ due to the difference in microstructures prior to the aging treatment. Vickers hardness, which is one indication of the material's response to the aging treatment, was found to have almost doubled in the heat-treated samples (Standard HSA, Modified HA and Aging only), as summarised in Fig. 10a. This shows that the aging treatments are largely responsible for the hardening effect, which is likely to be due to the precipitation of γ" particles in the matrix. In addition, measured hardness values are relatively uniform across the build height in all four samples (Fig. 10a).

Amongst the heat-treated samples there is a small variation in Vickers hardness values. The hardest at 434 HV is the Standard HSA sample, followed by Aging only at 411 HV, and the lowest is Modified HA at 392 HV. From the microstructures described in Section 3.2.1, the Modified HA material would be expected to have the best response to the aging treatment due to the lack of Laves or δ phases, which diminish available Nb for γ" precipitation. However, this was not reflected in the results and one possible explanation for this is described in Section 3.3.1. The higher hardness of the Standard HSA sample than the Aging only sample suggests that despite the precipitation of δ, the dissolution of Laves phase improves the material's response to aging.

The strengthening effects from the aging treatment can also be observed in the tensile properties of the materials, shown by the stress-strain curves in Fig. 10b. The yield strength ($YS_{0.2}$), obtained using 0.2% proof stress, and ultimate tensile strength (UTS) for all three heat-treated samples are at least 250 MPa higher than that of the As-Dep samples. However, the elongation (EL) of the Standard HSA and Aging only samples were just one-tenth that of the As-Dep samples. The poor elongation in the Standard HSA and Aging only

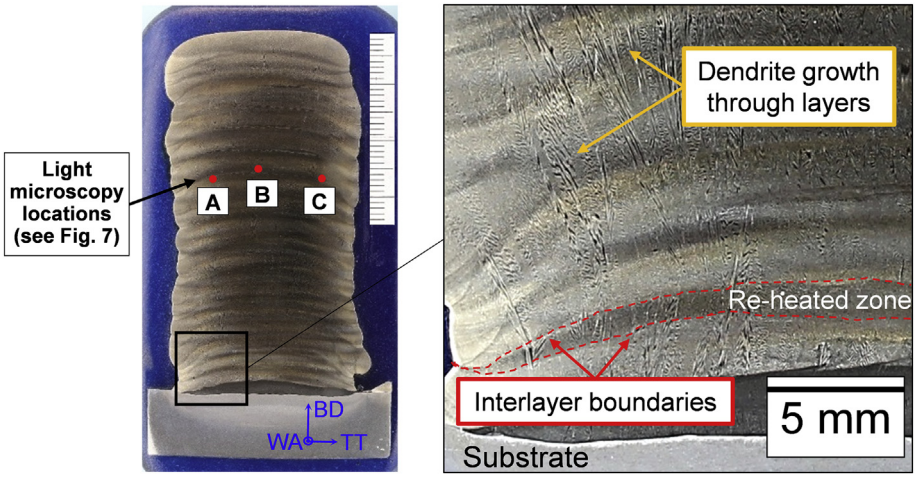


Fig. 6. Macrograph showing locations of light micrographs A, B, C in Fig. 7, dendritic features, re-heated zone and interlayer boundaries.

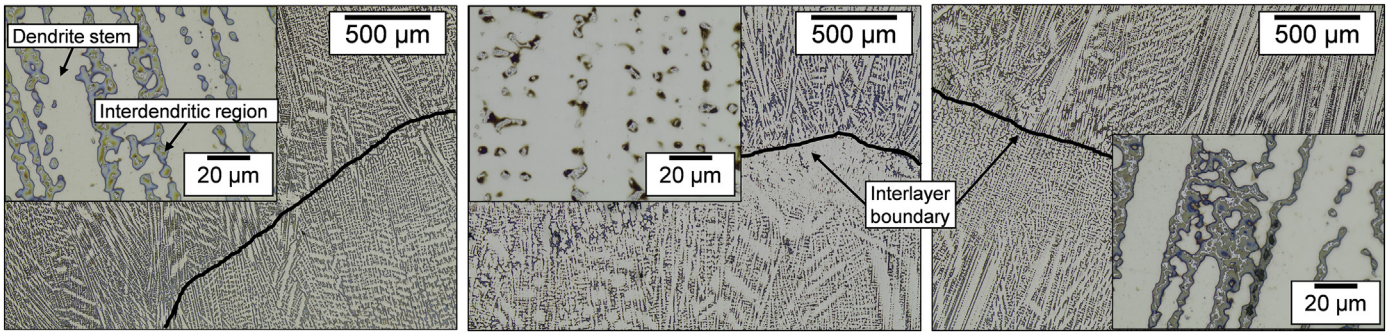


Fig. 7. Optical micrographs of As-Dep WAAM Inconel 718 material in the through-thickness section at locations shown in Fig. 6.

samples could be due to Laves and δ phases acting as stress concentrators in the precipitation-hardened matrix. Although the As-Dep material also contains Laves phase, its more ductile matrix may have compensated for the stress concentration effect. Overall, the Modified HA samples showed the best combination of $YS_{0.2}$, UTS and EL.

3.3. Direction dependence before and after heat treatment

3.3.1. Grain morphology and texture

Grains in the As-Dep sample were found to be columnar with long axis in the build direction. The grains are coarse, with length up to several mm, as shown in EBSD maps in Fig. 11a. Columnar grain structures have also been observed in materials built from other AM processes, such as selectively laser melted IN718 [41,42] and electron beam melted IN718 [43] and Ti-6Al-4V [44].

In the Modified HA sample, grains were found to have coarsened to more than three times the size of those in the As-Dep sample (Fig. 11b). Grain coarsening is likely to be a result of the high homogenisation temperature used in the Modified HA treatments. The grains retain some of their previous morphology, longer in the build direction than in the other directions. Equivalent grain diameters in the TT, WA and BD directions are shown in Table 2. The coarse grains in the Modified HA sample could be a reason for its lower hardness, YS and UTS compared to the Standard HSA and Aging only samples, as described in Section 3.2.2.

The As-Dep material has a strong fibre texture, indicated by the colouring of the EBSD maps (Fig. 11a) and pole figure (Fig. 12a). The colouring of the EBSD maps shows the strong crystallographic texture of the As-Dep material, where the grains have a preferential orientation in the build direction. The pole figure shows a high intensity in the centre of the figure, indicating that most of the grains have their ⟨100⟩ direction well-aligned with the build direction. The scattered intensity along the rim of the pole figure, indicates that the grains are randomly rotated about the build direction. In contrast, the texture of the Modified HA sample is weaker than that of the As-Dep sample, shown by the more random colouring of the EBSD maps in Fig. 11b and the scattered spots in Fig. 12b. The intensity of the spots in the latter is likely to be due to the large grain size and limited number of grains used in the analysis.

3.3.2. Tensile properties

3.3.2.1. Stress-strain curves. Tensile properties, from As-Dep and Modified HA materials in the build and wall axis directions, were obtained from the stress-strain curves shown in Fig. 13 and are summarised in Table 3. The As-Dep material displays weak direction dependency in tensile properties at room and elevated temperatures. Direction dependency manifests in UTS at room temperature, but in $YS_{0.2}$ at elevated temperature, both of which are higher in the build direction. These observations can be attributed to the columnar grains and fibre texture of the As-Dep material, as described in Section 3.3.1. Although the As-Dep samples displayed good ductility (EL of at least 9%), the scatter in the results is large.

The Modified HA material displays tensile properties with weak direction dependency at room temperature, and almost no direction dependency at elevated temperature. Direction dependency at room temperature manifests as a higher $YS_{0.2}$ in the wall axis direction. This could be due to the elliptical grain morphology and weak texture as described in Section 3.3.1. The UTS in both directions are relatively similar. At elevated temperature, direction dependency is greatly reduced, where the average $YS_{0.2}$ and UTS in each direction differ by not >21 MPa. The Modified HA material is also less ductile at elevated temperature than at room temperature, indicated by the poorer elongation. The extent of anisotropy for both the As-Dep and Modified HA materials is described in Section 3.3.2.2. A comparison of the measured tensile properties with those from conventional material are shown and discussed in Section 4.5.

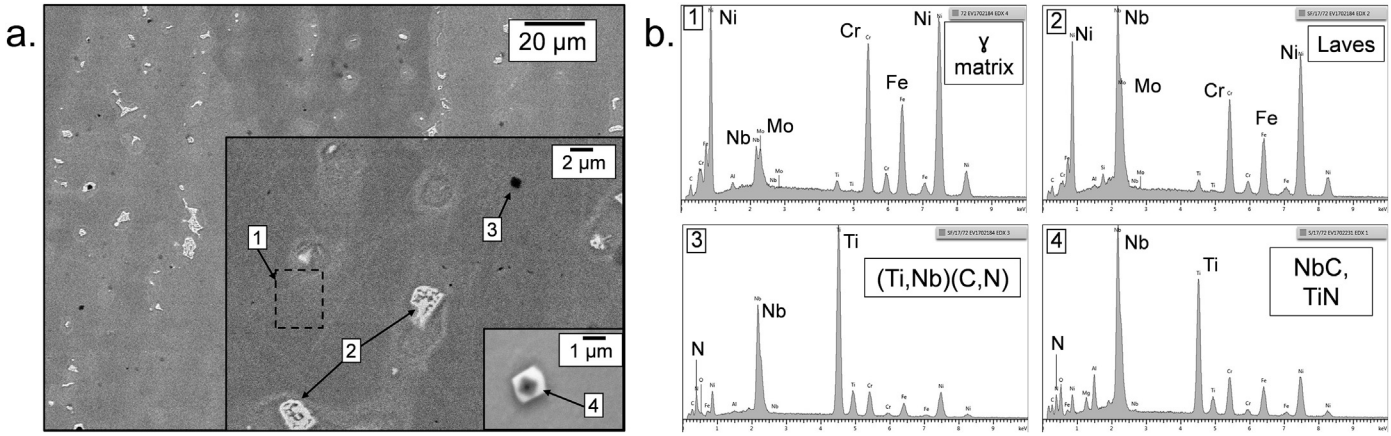


Fig. 8. As-Dep WAAM Inconel 718 material (a) backscatter electron images and (b) corresponding EDX spectra of spot analysis.

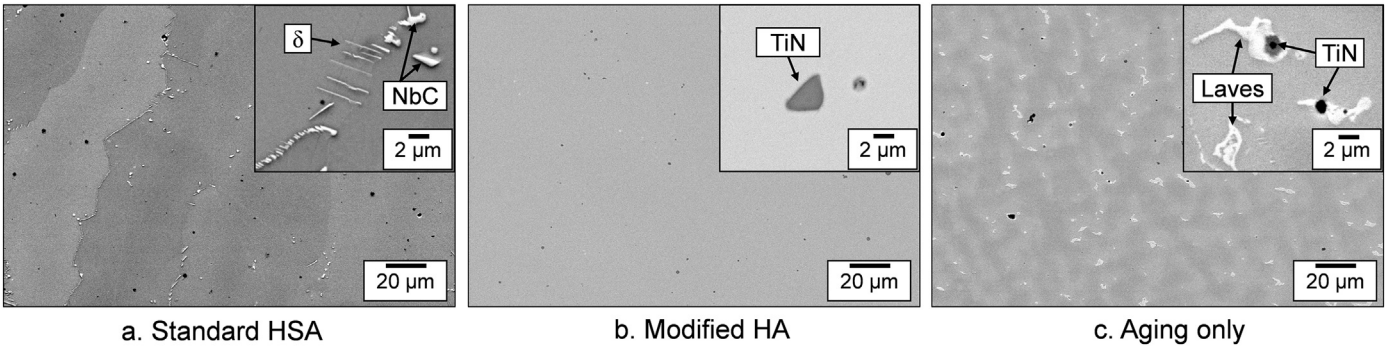


Fig. 9. Backscatter electron images of WAAM IN718 after (a) Standard HSA, (b) Modified HA and (c) Aging only heat treatments.

Dynamic strain aging (DSA) behaviour was observed to be more extensive in the Modified HA material than in the As-Dep material, indicated by early onset of the serrations in the stress-strain curves shown in the insert of Fig. 13b. DSA behaviour, which occurs when diffusing solute atoms and mobile dislocations interact, can be influenced by hardening precipitates γ" in wrought IN718 [46], and has been observed in electron beam melted IN718 containing γ" [47]. In addition, the unique fibre texture of the As-Dep material could also have contributed to the absence of DSA behaviour, which has been observed in laser deposited IN625 [48].

3.3.2.2. The extent of anisotropy. The extent of anisotropy can be represented as a ratio of the material properties in one direction over the properties in another. The further the property ratio is from 1, the more anisotropic the material is. The property ratio, *R*, for $YS_{0.2}$, is given by $R_{\sigma_{YS}} = \sigma_{YSWA}/\sigma_{YSBD}$, where σ_{YS} refers to $YS_{0.2}$ and subscripts WA and BD refer to wall axis and build direction respectively. *R* for YS and UTS of the As-Dep and Modified HA materials at room and elevated temperatures, is shown in Fig. 14. For comparison, tensile properties of WAAM IN718 reported by Xu et al. [10] have also been included.

The *R*-values shown in Fig. 14 are relatively close to 1, indicating that the tensile properties (YS and UTS) of WAAM IN718 material are only weakly anisotropic. The As-Dep materials displayed *R*-values furthest from 1, with the largest at 1.236 (As-Dep RT Wire B [10]), and smallest with 0.855 (As-Dep RT and As-Dep 650). From this, it can be concluded that the YS and UTS of As-Dep material in the wall axis direction is at least 0.85 that of the build direction. Of the heat-treated materials (i.e. Modified HA and Standard STA [10]), the Modified HA material displayed almost isotropic properties at elevated temperature, with *R*-values for both YS and UTS closest to 1.

4. Discussion

4.1. Laves phase mitigation

Despite the presence of Laves phase in the microstructure (as described in Section 3.1.2), the As-Dep material displayed good tensile properties comparable to equivalent conventional material (discussed in Section 4.5). However, poor elongation was observed in the Aging only tensile sample (reported in Section 3.2.2), which has been attributed to the embrittling effect of Laves phase within a precipitation-hardened matrix. Therefore, if WAAM IN718 material is to be used in a precipitation-hardened condition, post-deposition heat treatments should include a suitable homogenisation heat treatment to address Laves phase prior to precipitation hardening.

Further, the effectiveness of the homogenisation treatment may be dependent on the size and distribution of Laves phase in the As-Dep microstructure. As described in Section 3.3.1, the use of a high homogenisation temperature designed to address Laves phase has led to undesirable grain coarsening. Mitigating the formation of Laves phase during deposition could help in the design of homogenisation heat treatments to dissolve Laves phase without significant grain coarsening. This can be achieved by lowering the homogenisation treatment temperature and shortening the hold time, or both. For example, Laves phase dissolution was achieved in electron beam weld fusion zones with a 980 °C, 1 h solution treatment [26] and selective laser melted samples with 1180 °C, 15 min

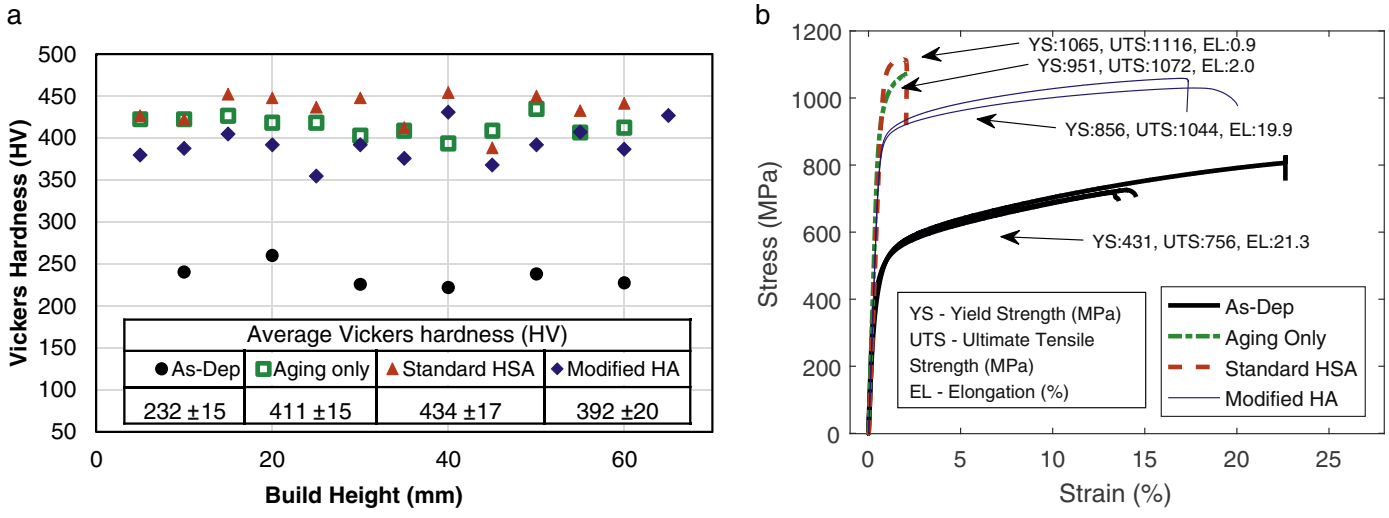


Fig. 10. (a) Vickers hardness with increasing build height and a summary of the average and standard deviation, and (b) engineering stress-strain curves from samples loaded in the build direction at room temperature.

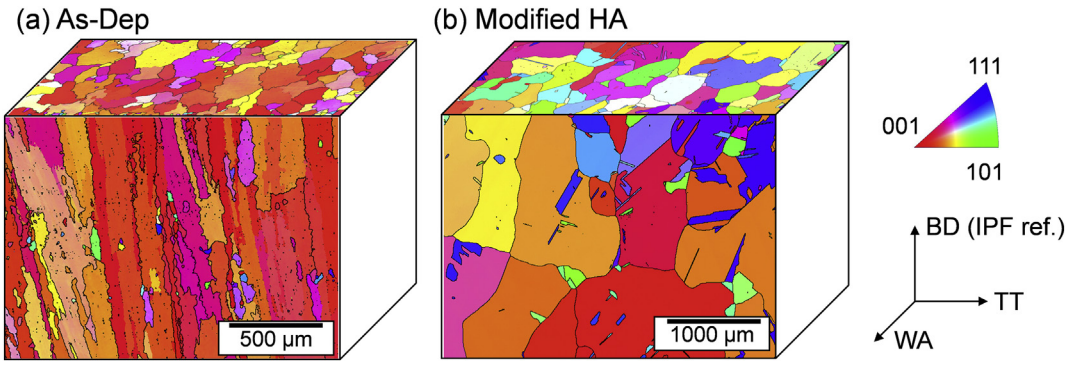


Fig. 11. Inverse pole figure EBSD maps of (a) As-Dep and (b) Modified HA materials, with IPF colouring reference in BD showing high angle (>15°) grain boundaries.

Table 2
Average grain diameters for as-deposited and modified solution aged material, measured using line intercept method [45].

	Average grain size (μm)	
	As-Dep	Modified HA
TT	76.9 ± 24.0	365.4 ± 91.8
WA	93.8 ± 29.6	297.2 ± 109.9
BD	250.0 ± 365.2	766.7 ± 200

homogenisation treatment [49], as both materials (in the as-welded/as-deposited condition) had finer and more sparsely distributed Laves phase than As-Dep WAAM IN718 material. In addition, partial dissolution of Laves phase was achieved in laser powder fed additively manufactured IN718 [50] with 1050 °C, 15 min homogenisation treatments, which changed the morphology of Laves from long striped to granular, thereby improving the tensile properties of the material.

Although it is difficult to monitor and control the thermal conditions during deposition, strategies have been adopted in welding to mitigate the formation of Laves phase. In arc welding, the use of pulsed as opposed to continuous current sources have been found to produce weld fusion zones with smaller and less densely distributed Laves phase particles [38,51], due to decreased heat input. Further, increasing weld cooling rates have been shown to decrease the segregation of Nb in the weld fusion zone [52]. Adopting these techniques in WAAM may help in minimising the formation of Laves phase in the as-deposited microstructure.

4.2. Role of δ phase in ductility

It has been assumed that the presence of δ phase in a precipitation-hardened matrix was largely responsible for poor elongation in the Standard HSA sample (reported in Section 3.2.2). The possibility of poor elongation being caused by other factors such as defects is small, as all other tensile samples with loading axis in the build direction (except the Aging only sample, discussed in Section 4.1), displayed elongation above 5%. Nonetheless, the effect of δ phase on mechanical properties is largely debated in the literature and is often discussed in the context of hot working formability [53,54], where ductility prior to precipitation hardening is of more interest. It is generally accepted that large amounts of δ phase deplete the matrix of Nb for γ" precipitation, which results in a decrease in strength. However, in the range of 0.3 to 1.4% volume fraction, δ phase has been found to have no effect on the yield and ultimate tensile strength, but decreased ductility by up to 10% in precipitation-hardened IN718 [36]. Apart from tensile properties, δ phase also has effects on stress rupture and creep properties. In wrought IN718 samples without δ phase, the stress rupture life and creep elongation to failure was found to be twice and four to five times those containing δ phase [55]. Whilst it is specified in AMS5662 [22] that the presence of Laves phase within the microstructure is not acceptable, that of δ depends on specific requirements. Owing to the complex effects of δ phase on mechanical properties, heat treatment strategies for WAAM IN718 material should be designed with careful consideration of the effects of δ phase.

4.3. Grain structure–tensile property relationship

Despite the columnar and elliptical grain morphology of the As-Dep and Modified HA materials (described in Section 3.3.1), the tensile properties of both materials (Section 3.3.2) do not appear to be significantly direction dependent. Although this observation has been reported in another study [10] of WAAM IN718 material, the reasons behind this observation remain unclear. For the As-Dep material, it would be expected that both the grain shape and fibre texture would contribute to anisotropic tensile properties. For the Modified HA material, contributions from the elliptical grain shape would be expected to be higher given the reduced texture. Nonetheless, the property ratios for both the As-Dep and Modified HA

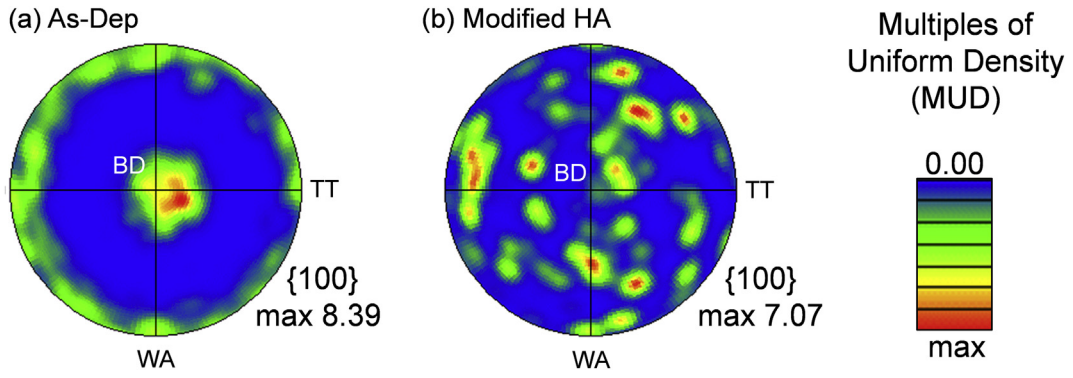


Fig. 12. Pole figures of (a) As-Dep and (b) Modified HA materials, determined from EBSD.

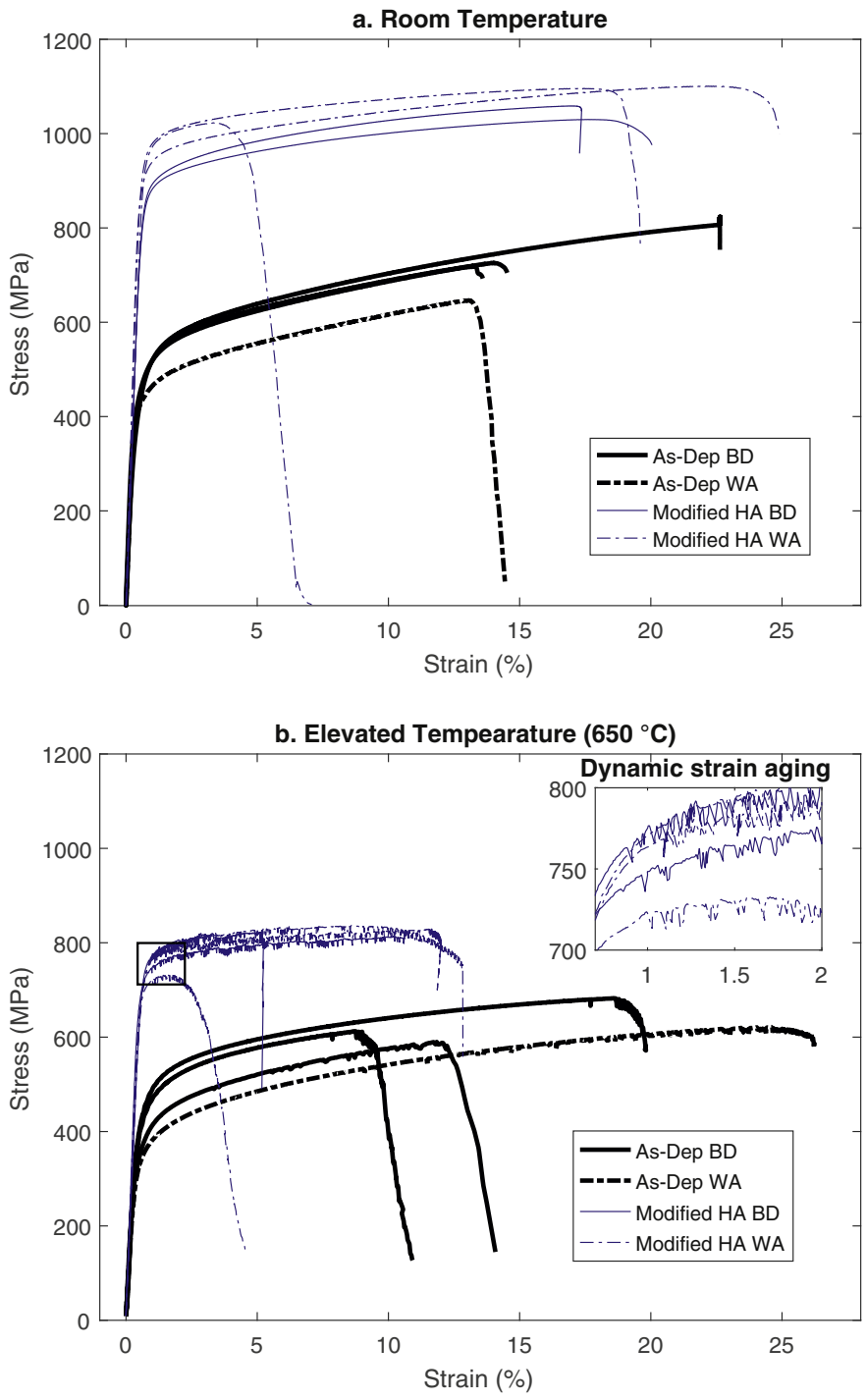


Fig. 13. Engineering stress-strain curves of As-Dep and Modified HA tensile specimens loaded separately in the build and wall axis directions (BD and WA respectively), at (a) room and (b) elevated temperature (650 °C).

materials as described in Section 3.3.2.2 were found to be close to 1, indicating that the relationship between grain structure and tensile properties is indirect.

4.4. Tensile fracture surface morphology

Ductile fracture was observed to be the main failure mechanism of the As-Dep and Modified HA tensile samples, which is consistent with the observed tensile properties described in Section 3.3.2.1. This is evidenced by the dimples observed on the fracture surfaces of the samples, shown in Fig. 15a, which are characteristic of microvoid coalescence. The As-Dep and Modified HA samples tested at both room and elevated temperatures, displayed similar dimple morphology at high magnification. Particles within the dimples were found to be rich in Nb. Given their size (~1 μm), they are likely to be either Nb-rich carbides or Laves phase (for the As-Dep material). At a lower magnification, a difference in dimple patterns was observed between the samples loaded in the wall axis and build directions, as shown in Fig. 15b and c. The former displays dimples neatly arranged in rows much like the interdendritic patterns shown in Fig. 7b, whereas the latter displays dimples in a random pattern. This implies that microvoids have initiated at inhomogeneities in the microstructure, such as carbides, nitrides and Laves phase, as described in Section 3.1.2. As these inhomogeneities tend to form in

Table 3
Summary of tensile properties.

	Room temperature						Elevated temperature (650 °C)			
	As-Dep		Aging only	Standard HSA	Modified HA		As-Dep		Modified HA	
Loading direction	BD[a]	WA[a]	BD	BD	BD	WA	BD	WA	BD	WA
UTS (MPa)	756 ± 47	646	1072	1116	1044 ± 14	1073 ± 36	628 ± 39	621	821 ± 2	800 ± 51
$YS_{0.2}$ (MPa)	431 ± 39	421	951	1065	856 ± 6	932 ± 2	395 ± 38	338	734 ± 18	720 ± 21
EL (%)	21.3 ± 7	17.7	2.0	0.9	19.9 ± 1	21.1 ± 8	9.0 ± 3	13.9	6.7 ± 3	5.9 ± 3

[a] BD and WA refer to build direction and wall axis respectively.

the interdendritic region, their distribution probably resulted in the patterns observed in Fig. 15b and c, and may be a contributing factor to the weakly anisotropic tensile properties of WAAM materials.

4.5. Comparison of tensile properties with conventional materials

The overall tensile performance of WAAM IN718 can be judged by comparison with conventional material. For the As-Dep material, a reasonable comparison would be all-weld-metal properties in the as-welded condition, and for the Modified HA material, precipitation hardened cast (AMS 5383 [16]) and wrought (AMS 5662 [22]) materials. The respective tensile properties are shown in Table 4.

At room temperature, the As-Dep material is weaker and less ductile than as-welded IN718, likely due to the coarser grains and more extensive Laves phase distribution in the former. The Modified HA material exceed the minimum specifications for cast IN718, not that of wrought IN718. One contribution to the inferior YS and UTS of the Modified HA material is its large grain size (described in Section 3.3.1) as compared to the maximum grain size allowable in AMS 5662 [22] (ASTM 2). At elevated temperature, tensile properties of the Modified HA material do not meet the minimum specified for wrought IN718. As AMS 5383 [16] does not specify minimum tensile properties for elevated temperatures, reported results from IN718 castings [56] were used instead for comparison. The YS and UTS of the Modified HA material exceeded that of the castings, but EL did not.

Considering that IN718 is most commonly used at elevated temperatures, the tensile properties of WAAM IN718 material are insufficient to replace conventional wrought material like for like. Whilst post-deposition heat treatments can improve the tensile properties from the As-Dep condition, the properties after a Modified HA treatment remain lower than the minimum specifications for wrought IN718. Although there is potential in optimising the temperature and hold time of the post-deposition homogenisation treatment to achieve finer grains which may improve tensile properties, the As-Dep microstructure provides an unfavourable starting point for improvement of mechanical properties through post-deposition heat treatments to the same level as conventional wrought material. Nonetheless, post-deposition heat treatments are crucial in optimising the mechanical properties of WAAM IN718 material.

5. Conclusions

The following conclusions can be drawn from this work:

i. As-deposited Wire + Arc Additive Manufactured IN718 material has a dendritic microstructure containing Laves phase, Ti- and Nb-rich inclusions. The presence of Laves phase provides evidence for the occurrence of micro-segregation during the deposition process.
ii. A standard aging treatment does not dissolve Laves phase into solid solution. A standard homogenisation and solution treatment dissolves Laves phase, but precipitates acicular δ phase at the grain boundaries. A modified homogenisation treatment was found to achieve dissolution of Laves phase without precipitating δ. Ti-and Nb-rich inclusions seem to be largely unaffected by the heat treatments.
iii. The as-deposited material has columnar grains with long axis in the build direction and displays a fibre texture, where

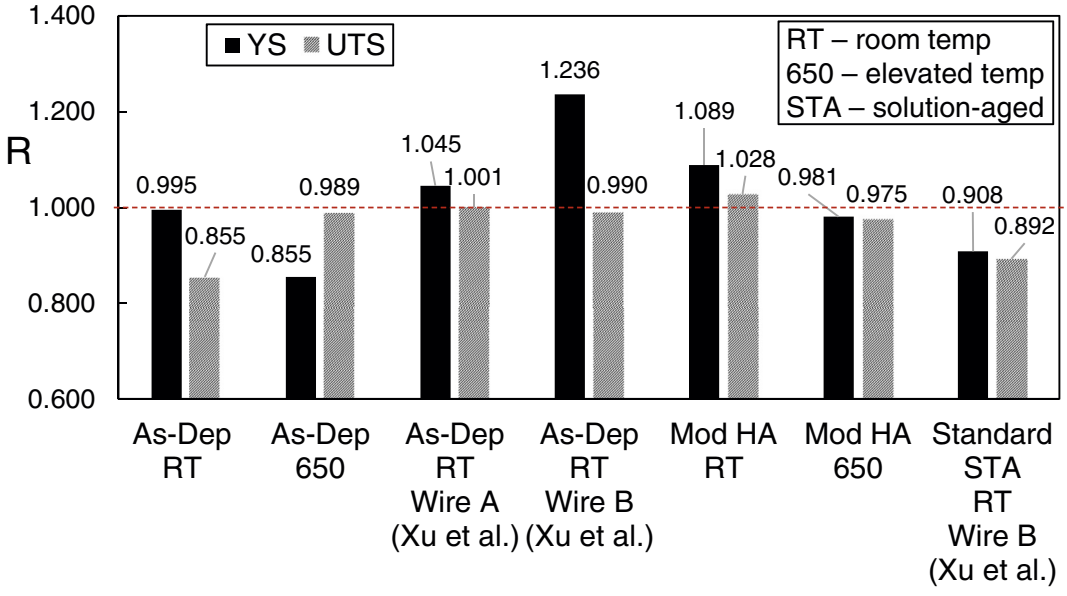


Fig. 14. Property ratios for yield strength (YS) and ultimate tensile strength (UTS) of WAAM IN718 materials from this work and reported values from Xu et al. [10].

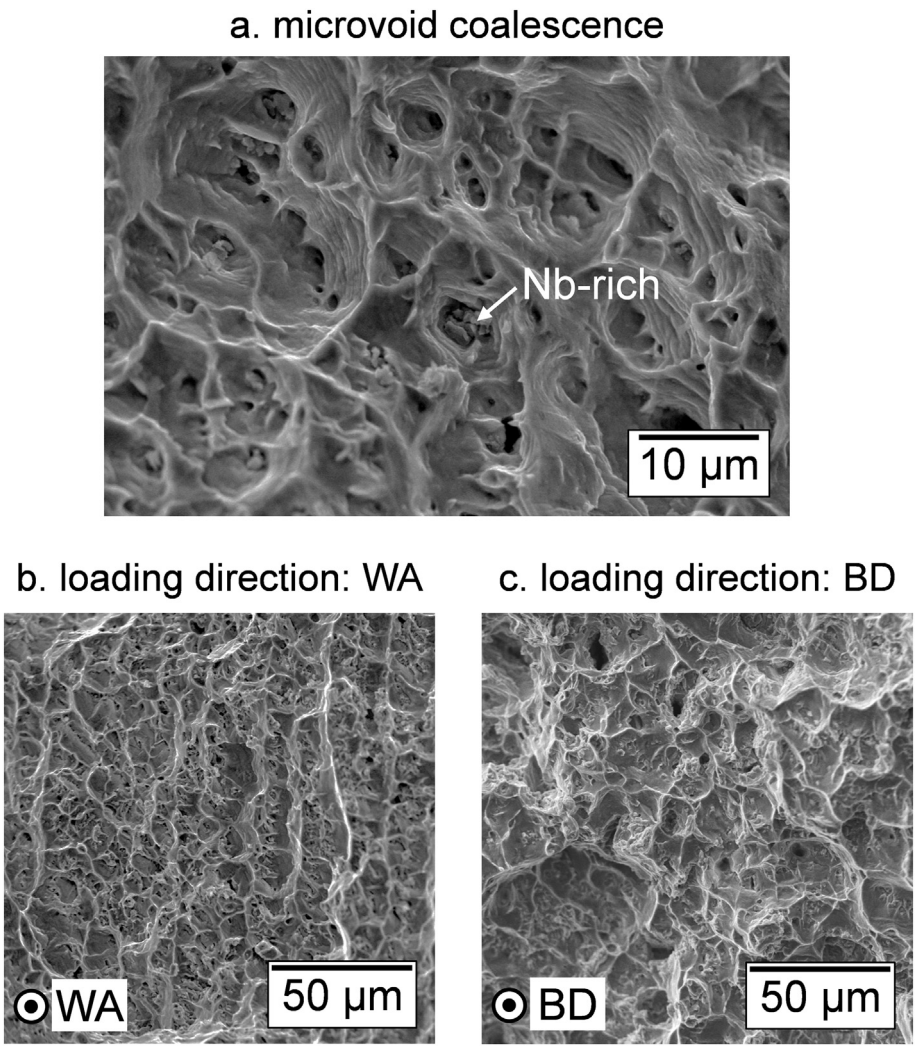


Fig. 15. Secondary electron images of fracture surfaces from tested tensile specimens (stress strain curves in Fig. 13), showing (a) dimples indicating microvoid coalescence characteristic of ductile fracture, and differences in dimple patterns observed in fracture surfaces normal to (b) wall axis and (c) build directions.

the ⟨100⟩ direction is preferentially aligned with the build direction. The grain size of modified homogenised and aged material is almost three times larger than in the as-deposited state and displays a weaker texture.

iv. As-deposited WAAM IN718 displays weakly anisotropic properties at room and elevated temperatures. The yield and ultimate tensile strengths measured perpendicular to the build direction are at least 0.85 of that parallel to the build direction. Modified homogenised and aged WAAM IN718 material displays weakly anisotropic properties at room temperature, but almost isotropic tensile properties at elevated temperature.

Declaration of competing interest

None.

CRediT authorship contribution statement

Cui E. Seow: Investigation, Data curation, Writing - original draft, Visualization.**Harry E. Coules:** Conceptualization, Writing - review & editing, Supervision, Funding acquisition.**Guiyi Wu:** Conceptualization, Writing - review & editing, Supervision, Funding acquisition.**Raja H.U. Khan:** Conceptualization, Methodology, Supervision.**Xiangfang Xu:** Resources.**Stewart Williams:** Resources.

Table 4
Comparison of tensile properties with equivalent conventional materials.

Condition	Room temperature					Elevated (650 °C) temperature			
	As-Dep[a]	As-welded[b]	Modified HA[a]	Cast[c]	Wrought[d]	As-Dep[a]	Modified HA[a]	Cast[e]	Wrought[d]
UTS (MPa)	729 ± 63	833	1062 ± 32	827	1241	627 ± 34	808 ± 38	576	1000
$YS_{0.2}$ (MPa)	430 ± 6	565	901 ± 41	724	1034	381 ± 41	726 ± 20	517	862
EL (%)	20.4 ± 6	28	20.7 ± 7	3	12	10.2 ± 3	6.2 ± 3	13.7	12

[a] Average of 4–5 tensile samples from both BD and WA directions.
[b] Reported values from tests of samples from manual gas tungsten arc process welded plates [57].
[c] Minimum values specified in AMS 5383 Table 3 [16].
[d] Minimum values specified in AMS 5662 Tables 2B and 3B [22].
[e] Reported results [56] from tests of castings homogenised at 1200 °C, 48 h followed by standard solution aging treatments.

Acknowledgements

The authors would like to thank Dr. Jialuo Ding and Flemming Nielsen for their assistance with sample manufacture. This project is jointly funded by the Lloyd's Register Foundation, the University of Bristol and TWI Ltd. The work was enabled through the National Structural Integrity Research Centre (NSIRC), a postgraduate engineering facility for industry-led research into structural integrity established and managed by TWI through a network of both national and international universities. HEC's contribution was funded by the UK Engineering and Physical Sciences Research Council (EPSRC) under grant no. EP/M019446/1. Lloyd's Register Foundation helps to protect life and property by supporting engineering-related education, public engagement and the application of research. www.lrfoundation.org.uk.

References

[1] ASTM International, ASTM F3187−16 Standard Guide for Directed Energy Deposition of Metals, ASTM International, West Conshohocken, PA, 2016.
[2] S.W. Williams, F. Martina, A.C. Addison, J. Ding, G. Pardal, P. Colegrove, Wire + arc additive manufacturing, Mater. Sci. Technol. 32 (7) (2016) 641−647.
[3] E.A. Loria, The status and prospects of alloy 718, JOM 40 (7) (1988) 36−41.
[4] M.J. Donachie, S.J. Donachie, Superalloys: A Technical Guide, 2nd edition, ASM International, 2002.
[5] M. Durand-Charre, J.H. Davidson, The Microstructure of Superalloys, Routledge, London, 2017.
[6] D. Clark, M.R. Bache, M.T. Whittaker, Shaped metal deposition of a nickel alloy for aero engine applications, J. Mater. Process. Technol. 203 (1−3) (2008) 439−448.
[7] D. Clark, M.R. Bache, M.T. Whittaker, Microstructural characterization of a polycrystalline nickel-based superalloy processed via tungsten-inert-gas-shaped metal deposition, Metall. Mater. Trans. B Process Metall. Mater. Process. Sci. 41 (6) (2010) 1346−1353.
[8] B. Baufeld, Mechanical properties of INCONEL 718 parts manufactured by shaped metal deposition (SMD), J. Mater. Eng. Perform. 21 (7) (2012) 1416−1421.
[9] G. Asala, A.K. Khan, J. Andersson, O.A. Ojo, Microstructural analyses of ATI 718Plus® produced by wire-ARC additive manufacturing process, Metall. Mater. Trans. A 48 (9) (2017) 4211−4228.
[10] X. Xu, J. Ding, S. Ganguly, S. Williams, Investigation of process factors affecting mechanical properties of INCONEL 718 superalloy in wire + arc additive manufacture process, J. Mater. Process. Technol. 265 (2019) 201−209. Mar.
[11] C.R. Cunningham, J.M. Flynn, A. Shokrani, V. Dhokia, S.T. Newman, Invited review article: strategies and processes for high quality wire arc additive manufacturing, Additive Manufacturing 22 (2018) 672−686. Aug-.
[12] P.A. Colegrove, et al., Microstructure and residual stress improvement in wire and arc additively manufactured parts through high-pressure rolling, J. Mater. Process. Technol. 213 (10) (2013) 1782−1791.
[13] F. Martina, P.A. Colegrove, S.W. Williams, J. Meyer, Microstructure of Interpass rolled wire + arc additive manufacturing Ti-6Al-4V components, Metall. Mater. Trans. A 46 (12) (2015) 6103−6118. Dec.
[14] J. Donoghue, A.A. Antonysamy, F. Martina, P.A. Colegrove, S.W. Williams, P.B. Prangnell, The effectiveness of combining rolling deformation with wire-arc additive manufacture on β-grain refinement and texture modification in Ti-6Al-4V, Mater. Charact. 114 (2016) 103−114.
[15] X. Xu, S. Ganguly, J. Ding, C.E. Seow, S. Williams, Enhancing mechanical properties of wire + arc additively manufactured INCONEL 718 superalloy through in-process thermomechanical processing, Mater. Des. 160 (2018) 1042−1051. Dec.
[16] SAE International, AMS5383F Nickel Alloy, Corrosion and Heat-Resistant, Investment Castings 52.5Ni - 19Cr - 3.0Mo - 5.1Cb(Nb) - 0.90Ti - 0.60Al - 18Fe Vacuum Melted Homogenization and Solution Heat Treated, SAE International, 2018.
[17] M. J. Cieslak, G. A. Knorovsky, T. J. Headley, and A. D. Romig, Jr, "The solidification metallurgy of alloy 718 and other Nb-containing superalloys," Superalloys 718 Metall. Appl., pp. 59−68, 1989.
[18] M.J. Sohrabi, H. Mirzadeh, M. Rafiei, Solidification behavior and laves phase dissolution during homogenization heat treatment of Inconel 718 superalloy, Vacuum 154 (2018) 235−243. Aug.
[19] BSI, BS EN ISO 6507-1:2018 Metallic Materials. Vickers Hardness Test. Test Method, BSI, 2018.
[20] BSI, BS EN ISO 6892-1:2016 Metallic Materials — Tensile Testing Part 1: Method of Test at Room Temperature, BSI, 2016.
[21] BSI, BS EN ISO 6892-2:2018 Metallic Materials — Tensile Testing Part 2 : Method of Test at Elevated Temperature, BSI, 2018.
[22] SAE International, AMS5662N Nickel Alloy, Corrosion and Heat-Resistant, Bars, Forgings, and Rings 52.5Ni - 19Cr - 3.0Mo - 5.1Cb (Nb) - 0.90Ti - 0.50Al - 18Fe Consumable Electrode or Vacuum Induction Melted 1775 °F (968 °C) Solution Heat Treated, Precipitation-Hardenable, SAE International, 2016.
[23] A. Ho, H. Zhao, J.W. Fellowes, F. Martina, A.E. Davis, P.B. Prangnell, On the origin of microstructural banding in Ti-6Al4V wire-arc based high deposition rate additive manufacturing, Acta Mater. 166 (2019) 306−323. Mar.
[24] J.I. Goldstein, D.E. Newbury, J.R. Michael, N.W.M. Ritchie, J.H.J. Scott, D.C. Joy, SEM image interpretation, in: Scanning Electron Microscopy and X-Ray Microanalysis, Springer New York, New York, NY, 2018, pp. 111−121.
[25] R.G. Ding, Z.W. Huang, H.Y. Li, I. Mitchell, G. Baxter, P. Bowen, Electron microscopy study of direct laser deposited IN718, Mater. Charact. 106 (2015) 324−337.
[26] C. Radhakrishna, K. Prasad Rao, The formation and control of Laves phase in superalloy 718 welds, J. Mater. Sci. 32 (8) (1997) 1977−1984.
[27] C.C. Silva, H.C. de Miranda, M.F. Motta, J.P. Farias, C.R.M. Afonso, A.J. Ramirez, New insight on the solidification path of an alloy 625 weld overlay, J. Mater. Res. Technol 2 (3) (2013) 228−237. Jul.
[28] A. Mitchell, A.J. Schmalz, C. Schvezov, S.L. Cockroft, The precipitation of primary carbides in alloy 718, in: Superalloys 718, 625, 706 and Various Derivatives (1994), 1994, pp. 65−78.
[29] S.L. Cockcroft, T. Degawa, A. Mitchell, D.W. Tripp, A. Schmalz, Inclusion precipitation in Superalloys, in: Superalloys 1992, 1992, pp. 577−586.
[30] G.A. Knorovsky, M.J. Cieslak, T.J. Headley, A.D. Romig, W.F. Hammetter, INCONEL 718: A solidification diagram, Metall. Trans. A. 20 (10) (1989) 2149−2158.
[31] H.O. Pierson, Interstitial nitrides: Properties and general characteristics, in: Handbook of Refractory Carbides and Nitrides, William Andrew Publishing, 1996, pp. 181−208.
[32] C.I. Garcia, A.K. Lis, E.A. Loria, A.J. DeArdo, Thermomechanical processing and continuous cooling transformation behavior of IN-718, Superalloys 1992 (1992) 527−536.
[33] S. Benhadad, N.L. Richards, M.C. Chaturvedi, The influence of minor elements on the weldability of an INCONEL 718-type superalloy, Metall. Mater. Trans. A Phys. Metall. Mater. Sci 33 (7) (2002) 2005−2017.
[34] R. Vincent, Precipitation around welds in the nickel-base superalloy, Inconel 718, Acta Metall. 33 (7) (1985) 1205−1216.
[35] O.T. Ola, F.E. Doern, A study of cold metal transfer clads in nickel-base INCONEL 718 superalloy, Mater. Des. 57 (2014) 51−59. May.
[36] L.C.M. Valle, L.S. Araújo, S.B. Gabriel, J. Dille, L.H. de Almeida, The effect of δ phase on the mechanical properties of an Inconel 718 Superalloy, J. Mater. Eng. Perform. 22 (5) (2013) 1512−1518. May.
[37] H.E. Chandler, Heat treater's Guide: Practices and Procedures for Nonferrous Alloys, ASM International, 1996.
[38] G.D. Janaki Ram, A. Venugopal Reddy, K. Prasad Rao, G. Madhusudhan Reddy, Control of laves phase in Inconel 718 GTA welds with current pulsing, Sci. Technol. Weld. Join. 9 (5) (2004) 390−398.
[39] J. Li, et al., Microstructural evolution and mechanical properties of IN718 alloy fabricated by selective laser melting following different heat treatments, J. Alloys Compd. 772 (2019) 861−870. Jan.
[40] Z. Wang, K. Guan, M. Gao, X. Li, X. Chen, X. Zeng, The microstructure and mechanical properties of deposited-IN718 by selective laser melting, J. Alloys Compd. 513 (2012) 518−523. Feb.
[41] N. Nadammal, et al., Effect of hatch length on the development of microstructure, texture and residual stresses in selective laser melted superalloy Inconel 718, Mater. Des. 134 (2017) 139−150.
[42] V.A. Popovich, E.V. Borisov, A.A. Popovich, V.S. Sufiiarov, D.V. Masaylo, L. Alzina, Functionally graded Inconel 718 processed by additive manufacturing: crystallographic texture, anisotropy of microstructure and mechanical properties, Mater. Des. 114 (2017) 441−449. Jan.
[43] A. Strondl, R. Fischer, G. Frommeyer, A. Schneider, Investigations of MX and γ′/γ″ precipitates in the nickel-based superalloy 718 produced by electron beam melting, Mater. Sci. Eng. A 480 (1−2) (2008) 138−147.
[44] A.A. Antonysamy, J. Meyer, P.B. Prangnell, Effect of build geometry on the β-grain structure and texture in additive manufacture of Ti6Al4V by selective electron beam melting, Mater. Charact. 84 (2013) 153−168. Oct.
[45] ASTM E112-13, ASTM E112−13 Standard Test Methods for Determining Average Grain Size, ASTM International, West Conshohocken, PA, 2013.
[46] W. Chen, M.C. Chaturvedi, On the mechanism of serrated deformation in aged Inconel 718, Mater. Sci. Eng. A 229 (1−2) (1997) 163−168.
[47] H.J. Lee, H.K. Kim, H.U. Hong, B.S. Lee, Influence of the focus offset on the defects, microstructure, and mechanical properties of an Inconel 718 superalloy fabricated by electron beam additive manufacturing, J. Alloys Compd. 781 (2019) 842−856. Apr.
[48] A.M. Beese, Z. Wang, A.D. Stoica, D. Ma, Absence of dynamic strain aging in an additively manufactured nickel-base superalloy, Nat. Commun. 9 (1) (2018).
[49] W. Huang, J. Yang, H. Yang, G. Jing, Z. Wang, X. Zeng, Heat treatment of Inconel 718 produced by selective laser melting: microstructure and mechanical properties, Mater. Sci. Eng. A 750 (2019) 98−107. Mar.
[50] S. Sui, et al., The influence of laves phases on the room temperature tensile properties of Inconel 718 fabricated by powder feeding laser additive manufacturing, Acta Mater. 164 (2019) 413−427. Feb.
[51] G.D. Janaki Ram, A.V. Reddy, K.P. Rao, G.M. Reddy, Improvement in stress rupture properties of Inconel 718 gas tungsten arc welds using current pulsing, J. Mater. Sci. 40 (6) (2005) 1497−1500.
[52] S.G.K. Manikandan, D. Sivakumar, K. Prasad Rao, M. Kamaraj, Effect of weld cooling rate on Laves phase formation in Inconel 718 fusion zone, J. Mater. Process. Technol. 214 (2) (2014) 358−364. Feb.
[53] M. Anderson, A.-L.L. Thielin, F. Bridier, P. Bocher, J. Savoie, δ Phase precipitation in Inconel 718 and associated mechanical properties, Mater. Sci. Eng. A 679 (2017) 48−55. Jan.
[54] B. Hassan, J. Corney, Grain boundary precipitation in Inconel 718 and ATI 718Plus, Mater. Sci. Technol. 33 (16) (2017) 1879−1889.
[55] C.-M. Kuo, Y.-T. Yang, H.-Y. Bor, C.-N. Wei, C.-C. Tai, Aging effects on the microstructure and creep behavior of Inconel 718 superalloy, Mater. Sci. Eng. A 510−511 (2008) 289−294.
[56] T. Trosch, J. Strößner, R. Völkl, U. Glatzel, Microstructure and mechanical properties of selective laser melted Inconel 718 compared to forging and casting, Mater. Lett. 164 (2016) 428−431. Feb.
[57] Special Metals Corporation, INCONEL Alloy 718, Special Metals Corporation, 2007, pp. 1−28.



https://dspace.org/

Wire+Arc Additively Manufactured Inconel 718: Effect of post-deposition heat treatments on microstructure and tensile properties

Seow, Cui Er; Coules, Harry E.; Wu, Guiyi; Khan, Raja H. U.; Xu, Xiangfang ...

2019-08-24
Elsevier
https://doi.org/10.1016/j.matdes.2019.108157
Seow CE, Coules HE, Wu G, et al.., (2019) Wire+Arc Additively Manufactured Inconel 718: Effect of post-deposition heat treatments on microstructure and tensile properties. Materials and Design, Volume 183, December 2019, Article number 108157

Downloaded from a DSpace repository. https://dspace.org/